Effects of projectile break-up on fusion cross sections at energies near and above the Coulomb barrier: A case of incomplete fusion

Mohd. Shuaib,[1,*] Vijay R. Sharma,[2] Abhishek Yadav,[3] Manoj Kumar Sharma,[4] Pushpendra P. Singh,[5] Devendra P. Singh,[6] R. Kumar,[3] R. P. Singh,[3] S. Muralithar,[3] B. P. Singh,[1,†] and R. Prasad[1]

[1]*Nuclear Physics Laboratory, Physics Department, Aligarh Muslim University, Aligarh 202 002, India*
[2]*Departamento de Aceleradores, Instituto Nacional de Investigaciones Nucleares, Apartado Postal 18-1027,*
C.P. 11801 Ciudad de Mexico, Mexico
[3]*NP-Group Inter-University Accelerator Centre, New Delhi 110 067, India*
[4]*Physics Department, Shri Varshney College, Aligarh 202 001, India*
[5]*Department of Physics, Indian Institute of Technology, Ropar, Punjab 140 001, India*
[6]*Department of Physics, University of Petroleum and Energy Studies, Dehradun 248 007, India*

In the present work, the experimental studies of projectile break-up (incomplete fusion) at energies $\approx$ 4–7 MeV/nucleon have been performed by using offline γ-ray spectroscopy. The excitation functions of reaction residues populated in the ^{19}F + ^{175}Lu system via complete fusion and/or incomplete fusion processes were measured and analyzed within the framework of the statistical model code PACE4. The measured excitation functions of xn and pxn channels are found to be well reproduced by the predictions of PACE4, which clearly indicates the population of these residues, predominantly, via complete fusion processes. However, in the case of residues involving α particles in the exit channels, the experimentally measured cross sections are found to show a significant enhancement when compared with PACE4 predictions. This enhancement points toward the onset of incomplete fusion reactions at the studied range of energies and is found to be projectile energy dependent. Further, an attempt was made to study the influence of projectile (strongly bound) break-up on fusion cross sections, above the Coulomb barrier, within the framework of the universal fusion function, which is a benchmark function that does not depend on the system parameters. The experimental fusion function was deduced for the complete fusion (CF) cross section ($\sum \sigma_{CF} = \sum \sigma_{xn+pxn}^{expt}$) and total fusion (TF) cross section ($\sum \sigma_{TF} = \sum \sigma_{CF+ICF}^{expt}$) for three strongly bound projectiles ^{13}C, ^{16}O, and ^{19}F (present work) on different target nuclei and compared with the universal fusion function. Analysis of data indicates 10–35% complete fusion suppression above the barrier, indicating that it is essentially due to the prompt break-up (incomplete fusion) of the strongly bound projectiles. Moreover, the deduced complete fusion suppression factor for the present work shows a conspicuous exponential relation with the break-up threshold of the projectile.

I. INTRODUCTION

In recent years, considerable experimental and theoretical efforts have been made to understand the dynamics of incomplete fusion (ICF) reactions in the heavy-ion (HI) collisions at energies from near the Coulomb barrier to well above it [1–6]. A comprehensive study of HI collisions has always been an active area of research [4,5,7,8]. At these energies, the dominating nuclear reaction is expected to be the complete fusion (CF) process; however, recent experimental data [5,6] show a significant contribution of ICF processes at these energies (i.e., $\approx$4–7 MeV/nucleon), which triggered a resurgent interest to understand the dynamics of such reactions. The CF process corresponds to the fusion of the entire projectile [for which the input angular momenta (ℓ) associated with the system for fusion to occur is $<\ell_{crit}$] with the target nucleus. However, in

the case of ICF reactions, the fusion of the entire projectile with the target nucleus is hindered; as a result, the projectile breaks up into its constituents due to the disappearance of the so-called fusion pocket in the interaction potential, if the input angular momenta associated with the system $\ell > \ell_{crit}$. After the break-up of the projectile, the remnant flows in the forward direction undeviated with almost beam velocity. The first experimental observation of ICF events in HI interactions was reported by Britt and Quinton [9], where fast α particles [as projectile-like fragments (PLFs)] in massive transfer reactions were detected at $E_{lab} \geqslant 10.5$ MeV/nucleon. Since then, the ICF has been extensively studied and has been established as one of the competing modes of reaction at $E_{lab} \approx 4-10$ MeV/nucleon [10–13]. Later, the production of PLFs associated with the massive transfer reactions was also reported by Kauffman and Wolfgang [14]. Several theoretical models, viz., the break-up fusion model [15,16], the sum-rule model [17], the exciton model [18], the promptly emitted particles model [19], and the overlap model [20–23], a brief description of which is given elsewhere [24], have been proposed to explain the ICF

data. It may be pertinent to mention that the aforementioned models are found to explain only to some extent the ICF data at projectile energies > 10.5 MeV/nucleon, but fail to explain the ICF data at low projectile energies (i.e., $\approx 4-7$ MeV/nucleon) which is the energy range of interest in the present work. Because of the unavailability of any reliable theoretical model, the experimental study of ICF is still an active area of research. Some of the important signatures of ICF processes are (i) a higher production cross section over the statistical model predictions for the reactions involving α particles in the exit channel [24], (ii) fractional linear momentum transfer from the projectile to the target nucleus [25,26], (iii) entirely different spin distribution patterns for CF and ICF residues [27], and (iv) a broader angular momentum distribution associated with CF events than with ICF events [27]. In recent years some studies have been done on the dependence of the ICF component on entrance channel parameters, viz., (a) projectile energy, (b) input angular momenta, (c) α-Q value of the projectile (which corresponds to the α binding energy of the projectile), (d) entrance channel mass asymmetry, and (e) the Coulomb effect, at energies $\approx 4-7$ MeV/nucleon. However, such studies are limited only to a few projectile-target combinations and mostly for α-cluster beams like ^{12}C and ^{16}O. However, for better understanding of ICF reaction dynamics it is required to extend these investigations to include non-α-cluster beams and a large number of projectile-target combinations covering the periodic table.

Therefore, in order to understand the effect of projectile break-up on fusion cross sections at low energies, cross sections for the population of reaction residues via CF and/or ICF processes in the system ^{19}F $+$ ^{175}Lu have been measured at energies $\approx 4-7$ MeV/nucleon. The analysis of data was performed within the framework of the statistical model code PACE4 [28]. The ICF strength function F_{ICF}, which is a measure of the relative strength of ICF to the total fusion cross section, was deduced. An attempt was also made to study the effect of break-up on total fusion (TF) cross section (σ_{TF}) and on CF cross sections (σ_{CF}) using the benchmark curve called the universal fusion function (UFF) [29]. The present paper is organized as follows: A brief description of the experimental methodology is given in Sec. II, Sec. III deals with the details of the analysis of data and its interpretation, and in Sec. IV a summary of the present work is presented.

II. EXPERIMENTAL METHODOLOGY

The experiment to measure the excitation functions (EFs) of reaction residues populated in the ^{19}F $+$ ^{175}Lu system was carried out at the ion beam facility of the Inter University Accelerator Centre (IUAC), New Delhi, India. The ^{19}F^{+7} beam produced by the accelerator is allowed to focus on ^{175}Lu targets. An activation (stacked foil) technique followed by offline γ-ray spectroscopy was employed. The details of the experimental methodology are given in Ref. [30]; however, for the sake of completeness, important details are given here. Isotopically pure ^{175}Lu targets (thickness $\approx 1.0-1.5$ mg/cm^2) and aluminum catcher/energy-degrader foils (thickness $\approx 1.5-2.5$ mg/cm^2) were prepared by the rolling technique. To achieve the wide range of energy, an energy-degradation technique was
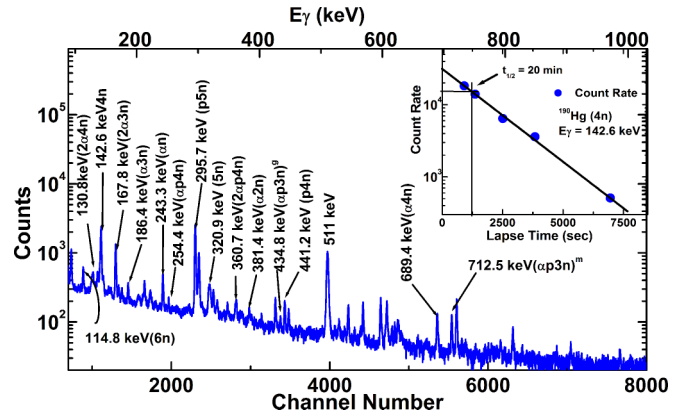

FIG. 1. A typical γ-ray spectrum of the ^{19}F $+$ ^{175}Lu interaction at 103.64 ± 1.36 MeV.

used in which each target foil is backed by an Al catcher foil (hereafter called the target-catcher assembly). In the present experiment, two stacks (one consisting of four target-catcher foil assemblies and the other of three target-catcher foil assemblies) were irradiated separately at 103.64 ± 1.36 and 108.54 ± 1.46 MeV beam energies. The irradiations were carried out in the General Purpose Scattering Chamber (GPSC) [31]. Considering the half-lives of interest, the irradiations were carried out for 8–10 h for each stack. The beam current was maintained at $\approx 25-30$ nA throughout the irradiations and was monitored using a Faraday cup installed downstream of the beam line. The activities induced were recorded separately at several time intervals using a single HPGe detector having 100 cm^3 active volume coupled to the CAMAC-based data acquisition system CANDLE [32].

III. ANALYSIS AND INTERPRETATION OF RESULTS

In order to measure the cross sections of reaction residues populated via CF and/or ICF at each studied energy, the residues were identified from the recorded γ-ray spectra by their characteristic γ-ray energies and further confirmed by the decay curve analysis. Here, each sample was counted many times to obtain the half-life of the residues. As a representative case, a typical γ-ray spectrum of the ^{19}F $+$ ^{175}Lu system (where most of the observed γ rays that were assigned to the different radioisotopes are labeled) recorded at energy 103.6 ± 1.3 MeV is shown in Fig. 1. Further, as a typical example, the decay curve of ^{190}Hg ($t_{1/2} = 20$ min) residues obtained by following the 142.6 keV γ line is also shown in the inset of Fig. 1, which is in good agreement with the literature value and confirms its identification. It may be pointed out that it is rather complicated and difficult to assign all the γ lines in the spectrum to the characteristic γ lines of CF and ICF residues; however, an attempt was made to assign the majority of the γ lines due to the residues of interest. Some of the residues are likely to be formed by the fusion-fission process of the completely and incompletely fused composite system as well [33]. The nuclear data like half-life, γ-ray energies, intensities, etc., of the identified reaction residues have been taken from

TABLE I. A list of identified reactions in the ^{19}F + ^{175}Lu system and their decay data.

Residue	Half-life	J^{π}	E_{γ} (keV)	I_{γ} (%)
^{190}Hg($4n$)	20 min	0^+	142.6	68
^{189}Hg($5n$)	7.6 min	$3/2^-$	320.9	8.01
^{188}Hg($6n$)	3.25 min	0^+	114.8	30
^{190}Au($p3n$)	42.8 min	1^-	295.7	71
^{189}Au($p4n$)	28.7 min	$1/2^+$	441.2	7.3
^{188}Au($p5n$)	8.84 min	1^-	265.6	34.7
^{189}Pt(αn)	10.87 h	$3/2^-$	243.3	7.0
^{188}Pt($\alpha 2n$)	10.2 d	0^+	381.4	7.5
^{187}Pt($\alpha 3n$)	2.35 h	$3/2^-$	186.4	16
^{186}Pt($\alpha 4n$)	2.0 h	0^+	689.4	70
^{187}Ir($\alpha p2n$)	10.5 h	$3/2^+$	177.6	56
^{186}Ir^g($\alpha p3n$)	16.64 h	5^+	434.8	33.9
^{186}Ir^m($\alpha p3n$)	2.0 h	2^+	712.5	2.8
^{185}Ir($\alpha p4n$)	14.4 h	$5/2^-$	254.4	13.3
^{183}Os($2\alpha 3n$)	13.0 h	$9/2^+$	167.8	8.8
^{182}Os($2\alpha 4n$)	22.1 h	0^+	180.2	33.5
^{181}Re($2\alpha p4n$)	19.9 h	$5/2^+$	360.7	56.0

the Table of Isotopes [34] and Nuclear Wallet card [35] and are listed in Table I.

After the identification of the reaction residues populated via CF and/or ICF, the production cross section (σ_r) was measured at each energy by using the standard formulation [36]. The uncertainties in the measured cross sections may arise due to several factors given in Ref. [6]. The overall error, including the statistical errors, is estimated to be $\leqslant 15\%$. The production cross sections of the reaction residues populated via CF and/or ICF processes and their comparison with the theoretical model predictions may provide information about the reaction mechanism involved. The experimentally measured EFs were analyzed within the framework of the statistical model code PACE4 [28], which is based on the Hauser-Feshbach theory of compound nucleus (CN) decay [37]. The details of the code are given in Refs. [6,28,30]. The code uses the statistical approach of CN deexcitation by Monte Carlo procedure. At each stage of deexcitation the angular momentum projections are calculated, which enables the determination of angular distributions of emitted particles, and angular momentum conservation is taken into account at each step. Gilbert and Cameron's nuclear level density parameter and spin cutoff parameter were adopted for the calculations [38] and the prescription of Kataria *et al.* [39] for the excitation energy dependence on the level density parameter were used in the code. The CF cross sections were calculated using the Bass model [40]. The transmission coefficients for neutrons and protons are calculated by using the optical model potentials of Becchetti and Greenlees [41], and the optical model potential of Satchler [42] is used for α-particle emission. In this code, the level density parameter $a(= A/K)$ is one of the most important parameters, where A is the mass number of the nucleus and K is a free parameter. The value of K may be varied to match the experimental data. It may be pertinent to mention that code PACE4 does not include the transfer and/or ICF channels; therefore, any enhancement in the experimental cross sections
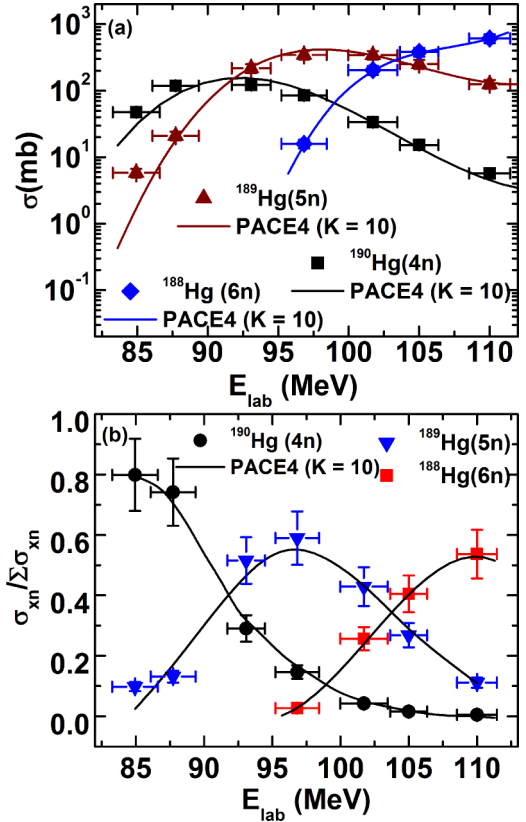

FIG. 2. (a) Experimentally measured EFs of ^{190}Hg, ^{189}Hg, and ^{188}Hg, residues populated via $4n$, $5n$, and $6n$, in the ^{19}F + ^{175}Lu system (see text for details). (b) Experimentally measured and theoretically calculated ratios of given complete fusion xn residues to the sum of all such residues for the ^{19}F + ^{175}Lu system.

as compared to the theoretical ones may be attributed to the incomplete fusion process.

A. Excitation function of *xn* and *pxn* channels: A comparison with PACE4

As discussed earlier, the EFs of reaction residues populated via CF and/or ICF processes were measured and compared with the theoretical predictions of PACE4 code at the studied range of energies. In the present work, the EFs for the reactions ^{175}Lu(^{19}F,$4n$)^{190}Hg, ^{175}Lu(^{19}F,$5n$)^{189}Hg, and ^{175}Lu(^{19}F,$6n$)^{188}Hg were measured and are shown in Fig. 2(a). In Fig. 2(b), the behavior of the individual EFs (xn-channels) with respect to the sum of cross-sections for xn channels ($\sum \sigma_{xn}$) is presented. As can be seen from this figure, the channels with successively larger numbers of neutron emissions become important as the energy of the incident beam increases. During the decay curve analysis, the cross section of reaction residues ^{190}Au($p3n$) having a half-life of 42.8 min was found to be strongly fed from its higher charge isobar precursor ^{190}Hg($4n$) having a half-life of 20 min, through β^+/EC decay. Therefore, to deduce the independent cross sections (σ_{ind}) of ^{190}Au, standard successive decay formulations proposed by Cavinato *et al.* [43] based on the Bateman equation [44] were
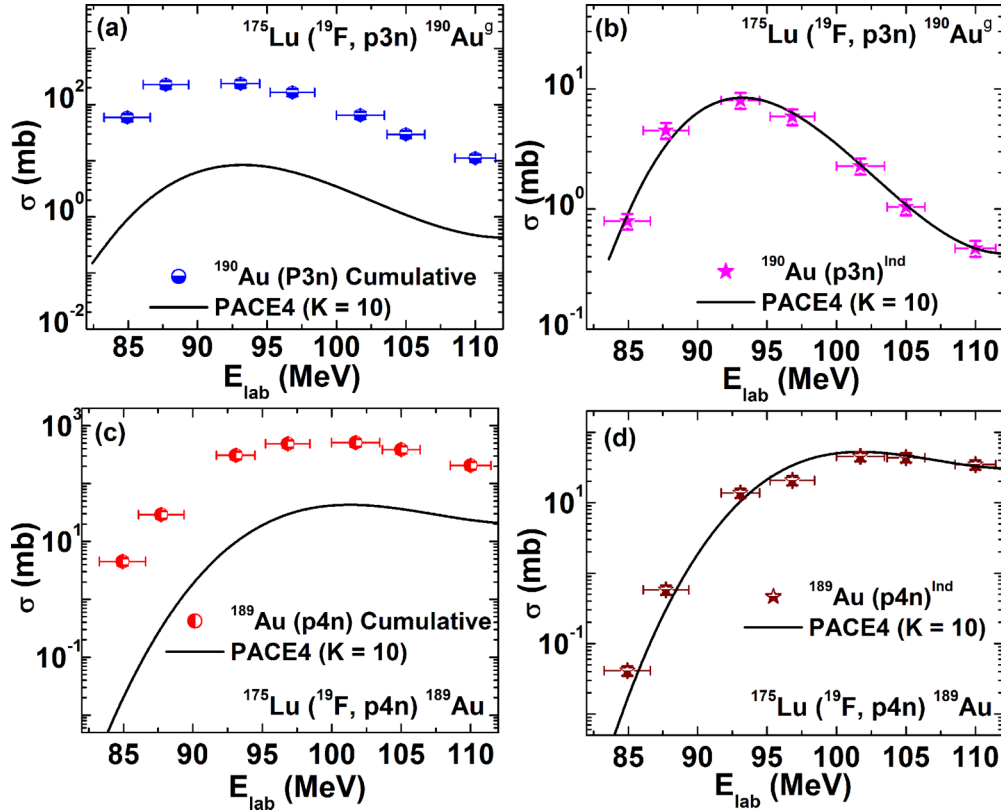
FIG. 3. Experimentally measured EFs of ^{190}Au and ^{189}Au residues populated via $p3n$ and $p4n$ channels compared with PACE4 calculations: (a) cumulative and (b) independent cross sections of ^{190}Au residues, and (c) cumulative and (d) independent cross sections of ^{189}Au residues (see text for details).

used and are given by the equation

$$\sigma_{\text{ind}} = \sigma_{\text{ind}} - P_{\text{pre}} \frac{t_{1/2}^d}{\left(t_{1/2}^d - t_{1/2}^{\text{pre}}\right)} \sigma_{\text{pre}}. \qquad (1)$$

In the above expression, $t_{1/2}^d$ and $t_{1/2}^{\text{pre}}$ are the half-lives of the daughter and precursor nuclei, respectively. The P_{pre} is the branching ratio of the decay from the precursor to its daughter nuclei. The values of half-lives and the branching ratio of the precursor decay (P_{pre}) are taken from Refs. [34,35]. The deduced independent production cross sections using the above formulation for the residues ^{190}Au are shown in Fig. 3(b). Similarly, using the above prescription, the independent production cross sections (σ_{ind}) were deduced for the residues ^{189}Au populated via the $p4n$ channel and presented in Fig. 3(d). Further, it may be pointed out that the EFs of other pxn channels could not be measured in the present work due to their short or long half-lives.

In order to understand the reaction mechanism involved in the production of evaporation residues populated via xn/pxn channels, an attempt was made to reproduce the experimentally measured EFs of these channels using the statistical model code PACE4. As can be seen from Fig. 2(a), the EFs for the xn channels are well reproduced by the PACE4 predictions for the level density parameter $a = A/10$ MeV^{-1}, indicating the production of these residues through the deexcitation of a fully equilibrated CN (^{194}Hg*) formed via the CF process. Further, as shown in Figs. 3(b) and 3(d), the deduced independent cross

section (σ_{ind}) of residues ^{190}Au($p3n$) and ^{189}Au($p4n$) are found to be in good agreement with the PACE4 predictions for the level density parameter $a = A/10$ MeV^{-1} and confirm the production of these residues via the complete fusion process. However, in Fig. 4, it may be pointed out that the evaporation residues ^{188}Au populated via the $p5n$ channel are also likely to be populated from its high-charge isobar; i.e., the precursor
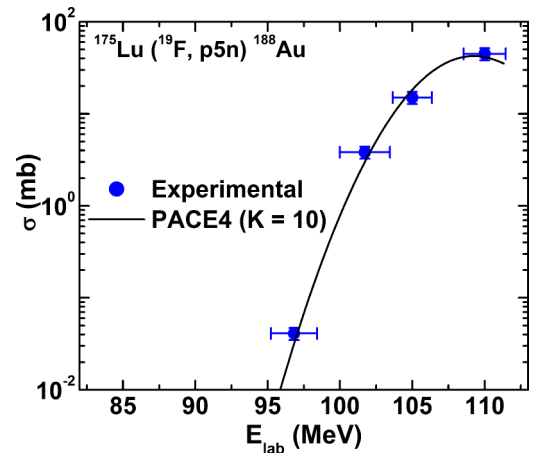

FIG. 4. Excitation function of reaction residues ^{188}Au populated via $p5n$ channel compared with PACE4 predictions (see text for details).
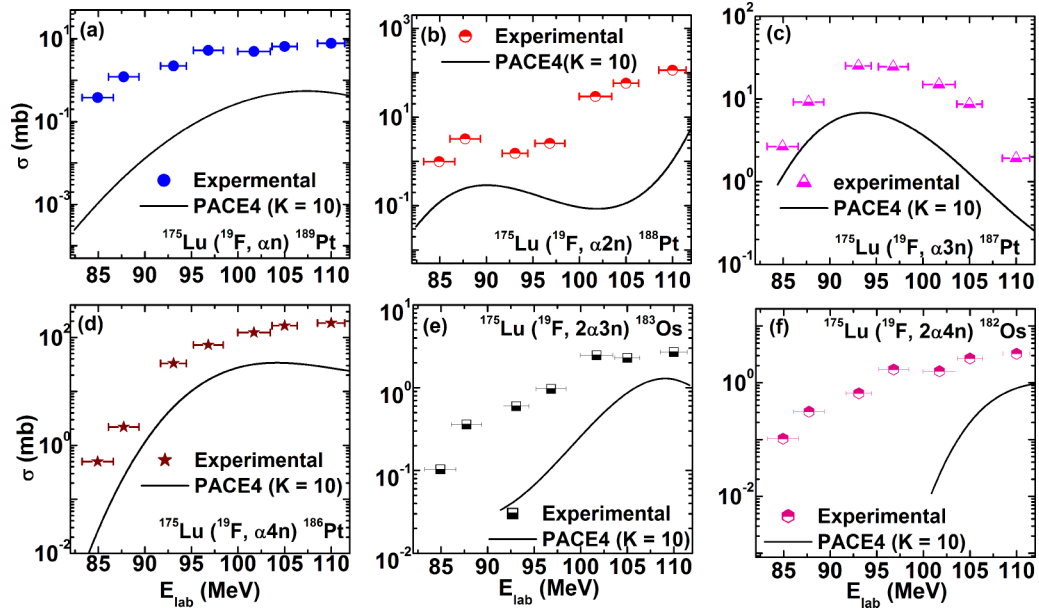
FIG. 5. Experimentally measured EFs of (a–d) ^{189,188,187,186}Pt (αxn, where $x = 1, 2, 3,$ and 4) and (e, f) ^{183,182}Os ($2\alpha xn$, where $x = 3, 4$) residues populated in the ^{19}F + ^{175}Lu system and compared with those calculated by the PACE4 model (see text for details).

decay of ^{188}Hg($6n$) through β^+/EC decay leads to the residues ^{188}Au. As can be seen from Fig. 4, the PACE4 code nicely reproduced the EFs of ^{188}Au($p5n$) and is well matched with the experimentally measured cross sections, which clearly indicates the negligible precursor contribution to this reaction channel, i.e., ^{175}Lu(^{19}F, $p5n$)^{188}Hg over the studied range of energy. Hence, the choice of parameters used for the analysis is appropriate, and therefore the value of the level density parameter, $a = A/10$ MeV^{-1}, is consistently used as a fixed parameter for all the channels expected to be populated via both CF and ICF processes.

B. Excitation function of α-emitting channels: Enhancement in the cross sections over the PACE4 predictions

Figures 5(a)–5(f) and 6(a)–6(d) show the EFs of ten identified evaporation residues ^{189,188,187,186}Pt (αxn), where $x = 1, 2, 3, 4$; $^{187,186g+m},^{185}$Ir (αpxn), where $x = 2, 3, 4$, and ^{183,182}Os ($2\alpha xn$), where $x = 3, 4$ and ^{181}Re^g ($2\alpha p4n$), respectively. It may be pointed out that, with the different choices of parameters of the statistical code, the explanation of production of all experimentally measured EFs of residues is quite easy, but from a physics point of view, it is unreasonable. Hence, in the present work all the calculations were performed with the same set of input parameters for all measured channels. It may be observed from Figs. 5 and 6 that the experimentally measured EFs of all the α channels show a significant enhancement as compared to the PACE4 calculations (solid black line curve) done with the same set of input parameters used to reproduce the EFs for xn and pxn channels (i.e., the level density parameter value is $a = A/10$ MeV^{-1}). As already mentioned, the PACE4 code does not take ICF into account; therefore, the experimentally observed higher production cross sections of the α-emitting channels with respect to the PACE4 calculations may be attributed to the ICF process. However, Fig. 6(d) shows the experimental EFs

of ^{181}Re^g ($2\alpha p4n$) residues, where the PACE4 code predicts the negligible cross sections indicating the production of the ($2\alpha p4n$) channel dominantly via ICF processes. Note that the residues involving α particle(s) in the exit channel may be populated from CF and/or ICF processes. In the case of CF, the fully equilibrated CN (^{194}Hg*), formed via the complete fusion of the projectile (^{19}F) with the target nucleus (^{175}Lu), deexcites by emitting the α-particle(s) in the exit channels. However, in the case of ICF, only a part of projectile (^{19}F → ^{15}N + α) fuses with the target nucleus (^{175}Lu), while remnant α or ^{15}N moves in the forward direction as a spectator. As a representative case, the residue ^{187}Pt can be populated in the following ways:

(i) via the CF of ^{19}F with ^{175}Lu,

$$^{19}\text{F} + {}^{175}\text{Lu} \Rightarrow {}^{194}\text{Hg}^* \Rightarrow {}^{187}\text{Pt} + \alpha 3n,$$
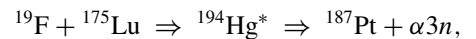
(ii) and when only a part of the projectile ^{19}F (i.e., ^{15}N) fuses with ^{175}Lu to form an incomplete fused composite system (^{190}Pt*), while an α-particle flows in the forward direction as a spectator. The excited ^{190}Pt* may then decay to ^{187}Pt via emission of three neutrons ($3n$) as ^{19}F(^{15}N + α) ⇒ ^{15}N + ^{175}Lu ⇒ ^{190}Hg* ⇒ ^{187}Pt + $3n$ ("α particle" as a spectator).

In order to deduce the contribution of ICF in all α channels, the data reduction procedure given in Ref. [10] was adopted and the ICF cross sections were deduced as $\sum \sigma_{\text{ICF}} = \sum \sigma_{\alpha xn+\alpha pxn+2\alpha xn+2\alpha pxn}^{\text{expt}} - \sum \sigma_{\alpha xn+\alpha pxn+2\alpha xn+2\alpha pxn}^{\text{PACE4}}$, i.e., by subtracting the PACE4 predictions for all α-emitting channels from their corresponding experimentally measured EFs at the studied range of energy. Recently, it was reported in our previous measurements of recoil range distributions [29,30] that the production of CF contributions in αxn channels are satisfactorily reproduced via PACE4 predictions done with the
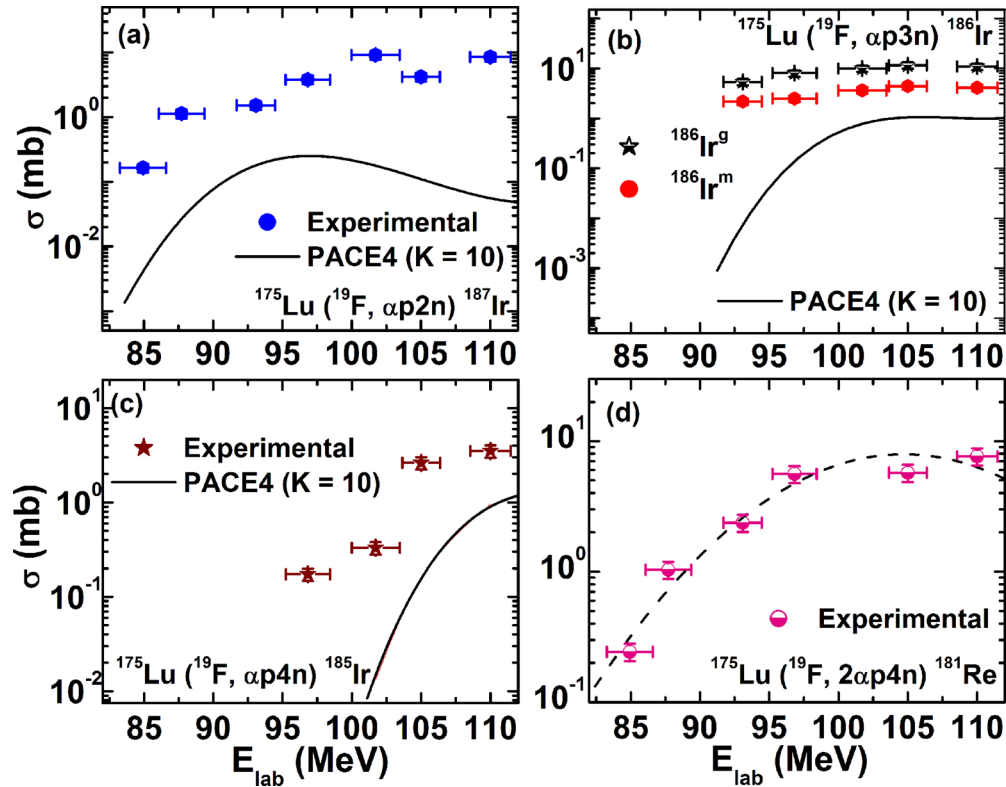
FIG. 6. Experimentally measured EFs of ^{187,186,185}Ir (αpxn, where $x = 2$, 3, and 4) and ^{181}Re($2\alpha p4n$) residues populated in the ^{19}F + ^{175}Lu system and compared with those calculated by the PACE4 model (see text for details). (d) The dashed line in the figure is to guide the eye.

same set of input parameters as used to calculate the cross sections of xn/pxn channels and gives a clear validation on the choice of PACE4 parameters as well as the present method of deducing the ICF contributions using the PACE4 predictions. Figure 7 shows the variation of total fusion cross sections
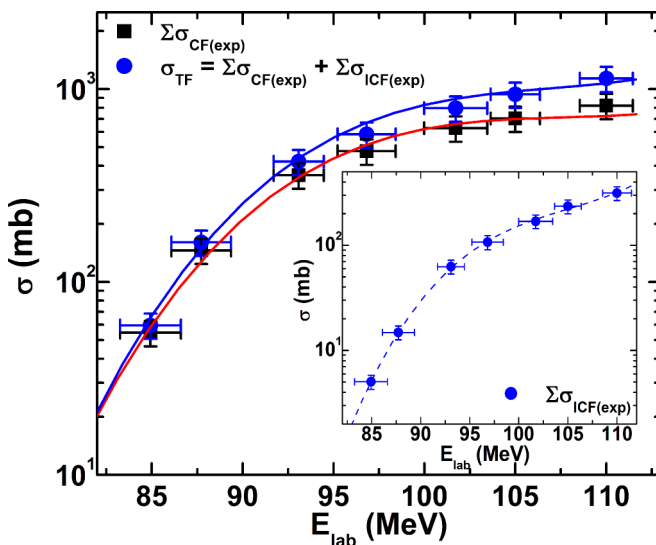

FIG. 7. The total fusion cross sections (σ_{TF}) and the sum of all CF channels (σ_{CF}), and (σ_{ICF}) cross sections (inset) are plotted as a function of incident projectile energy. Lines through the experimental data points are drawn to guide the eye.

(σ_{TF}) and the sum of all CF channels ($\sum \sigma_{CF}$) as a function of projectile energy. The contribution of ICF was deduced by subtracting the CF cross sections (σ_{CF}) from the measured total fusion cross sections (σ_{TF}) at the studied range of energy and is plotted in the inset in Fig. 7. As can be seen from this figure, that ICF cross section increases rapidly with beam energy, indicating its importance at relatively higher energies. It may be pertinent to mention that σ_{TF} has been corrected for those missing channels which could not be measured experimentally, by their corresponding PACE4 values.

C. Effect of projectile break-up on fusion cross section using the universal fusion function

In this section, an attempt was made to study the break-up effects of strongly bound projectiles (^{19}F, ^{16}O, and ^{13}C, having higher break-up threshold) on the fusion cross section at energies above the Coulomb barrier. As such the coupling effects excluding the break-up do not show their influence on the fusion cross section in this energy regime [45,46]. Therefore, to perform a systematic study of break-up effects on fusion cross sections in HI collisions involving strongly bound projectiles, it is necessary to select a standard reduction procedure that eliminates the geometrical effects [29,47] of the system, and data should be compared with the theoretical predictions without taking into account the coupling effect through the break-up channel. Several reduction procedures have been developed and are used to study the break-up effects [48–51]. Recently, Canto *et al.* [29,50] described a new

reduction procedure that completely eliminates the geometri-cal and static effects of the potential acting between the two nuclei. In this reduction procedure, the fusion cross section and the incident energy are reduced to a dimensionless equation called the fusion function $F(x)$ and dimensionless variable x:

$$\sigma_F \rightarrow F(x) = \frac{2E_{\text{c.m.}}}{\hbar \omega R_b^2}\sigma_F, \qquad (2)$$

$$x \rightarrow E_{\text{c.m.}} = \frac{(E_{\text{c.m.}} - V_b)}{\hbar \omega}, \qquad (3)$$

where $\hbar\omega$, R_b, and V_b are the barrier curvature, barrier radius, and barrier height while $E_{\text{c.m.}}$ is the collision energy in the center of mass, respectively. The above fusion function $F(x)$ is a dimensionless quantity associated with the fusion cross section, depending on a dimensionless variable x corre-sponding to the collision energy. As demonstrated by Sharma *et al.* [52], the barrier parameters are deduced by using the Wood-Saxon potential in which the diffuseness parameter was fixed to $a = 0.83$. The experimental fusion function $F(x)$ is obtained from the measured cross sections and from the barrier parameters using Eq. (2). It may be pointed out that some reduction procedures include only the radius and height of the fusion barrier. However, the transformation of Eqs. (2) and (3) considers the barrier curvature ($\hbar\omega$) as well, which has been overlooked so far in the literature [29,50]. This parameter is directly related to the tunneling probability and, therefore, plays a vital role at lower energies [50].

The reduction methods of Eqs. (2) and (3) are based on the famous Wong formula for the fusion cross section [29]:

$$\sigma_F^W = R_b^2 \frac{\hbar\omega}{2E_{\text{c.m.}}} ln\left[1 + \exp\left(\frac{2\pi(E_{\text{c.m.}} - V_b)}{\hbar\omega}\right)\right]. \quad (4)$$

It has been shown [29,45] that using the above approxima-tion in Eq. (2) the fusion function $F(x)$ reduces to

$$F(x) \rightarrow F_o(x) = ln[1 + \exp(2\pi x)]. \qquad (5)$$

Here, $F_o(x)$ is a general function of the dimensionless variable x and does not depend on the system properties. Therefore, for this reason it is called the universal fusion function [29]. It may be pointed out that Wong's formula for the fusion cross section is inaccurate at sub-barrier energies for light systems. However, the present work deals with incident energies much larger than the Coulomb barrier, where Wong's formula can be applied. As such, at $x > 1$, $F_0(x) \approx 2$. The fusion cross section reduces to Eq. (6), which signifies that fusion becomes independent of the width of the barrier and can be treated as the absorption by a black disk of radius R_b. The reduction in the CF flux due to break-up can be visualized as the partial fusion coming from one of the unfused parts of projectile, which is not falling into the black disk. Therefore, the UFF can be used as a benchmark curve to study the influence of break-up effects on fusion cross section.

Using the above reduction procedure, the deduced fusion functions of different systems can be compared directly with the UFF. Any deviation of fusion function from the UFF at energies above the Coulomb barrier may be attributed to the dynamical effects of projectile break-up on fusion cross
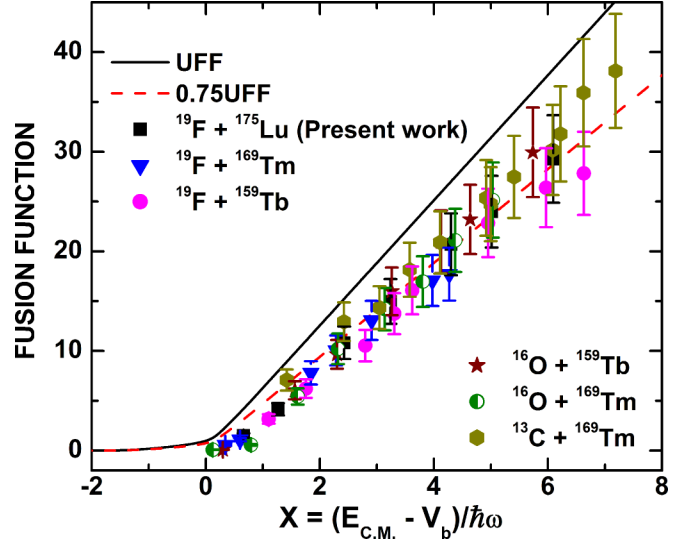

FIG. 8. The complete fusion function for strongly bound projec-tiles on different target nuclei. The solid black curve is the benchmark UFF. The dotted red line is the UFF multiplied by 0.75 (for details see text).

section:

$$\sigma_F = \pi R_b^2 (E_{\text{c.m.}} - V_b)/E_{\text{c.m.}}. \qquad (6)$$

In the present work, the experimental fusion functions are deduced for six systems, viz., ^{19}F + ^{175}Lu (in the present work), ^{19}F + ^{169}Tm [30], ^{19}F + ^{159}Tb [24], ^{16}O + ^{159}Tb, ^{169}Tm [53], and ^{13}C + ^{169}Tm [53], and are analyzed within the framework of the UFF. To understand the role of pro-jectile break-up on fusion cross sections, the experimental fusion functions for each of the above-mentioned systems was obtained for the complete fusion cross section (σ_{CF}) and for the total fusion cross section (σ_{TF}) and compared with the UFF. As already mentioned, at energies above the barrier, inelastic excitations and transfer channel couplings are not significant. Therefore, the difference in the experimental fusion function and UFF mainly arise from the break-up effects of the projectile on fusion cross section. The deduced CF fusion functions for strongly bound projectiles (^{13}C, ^{16}O, and ^{19}F) on different targets are plotted against the dimensionless parameter (x), illustrated in Fig. 8. The solid line represents the UFF, which is given by Eq. (5). As can be seen from this figure, the experimental fusion function for CF data is found to be 10–35% suppressed below the UFF owing to the prompt break-up of projectiles; i.e., some part of the flux has gone to the incomplete fusion reactions at the studied range of energies. As demonstrated in Ref. [54], a systematics between the suppression factor $\log(1 - F_{\text{B.U.}})$ and break-up threshold energy ($E_{\text{B.U.}}$) of the projectile was developed and it has been shown that the CF suppression factor is mainly determined by the break-up threshold of the projectiles. The CF suppression for the same projectile on different targets is also found to be independent of the target charge. Therefore, an attempt has been made to study the correlation between the CF suppression factor and break-up threshold energy for a more strongly bound projectile, i.e., ^{19}F ($E_{\text{B.U.}} = 4.01$ MeV) on three heavy target
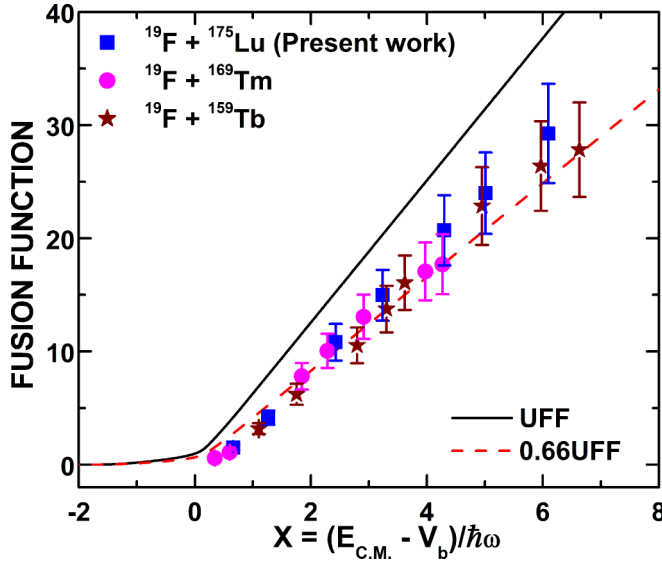
FIG. 9. The complete fusion function plotted separately for the ^{19}F projectile on different target nuclei, viz., ^{159}Tb, ^{169}Tm, and ^{175}Lu. The solid black curve is the benchmark UFF. The dotted red line is the UFF multiplied by 0.66 (for details see text).

nuclei, viz., ^{159}Tb, ^{169}Tm, and ^{175}Lu, which may give more strength to the systematics developed by Wang *et al.* [54]. The experimental CF function for three systems, viz., ^{19}F + ^{175}Lu (in the present work), ^{19}F + ^{159}Tb [24], and ^{19}F + ^{169}Tm [30], is shown separately in Fig. 9. The lowest break-up channel for ^{19}F is ^{19}F $\rightarrow$ ^{15}N + α with a threshold energy of 4.01 MeV. From Fig. 9, as expected the CF function is found to be suppressed below the UFF line, which is attributed to the break-up effects on fusion cross section. The experimental CF function coincides with the UFF scaled by the $F_{B.U.}$ of 0.66, which is displayed by the dotted line. Further, it may be pointed out that CF suppression is found to be almost independent of the target charge. The suppression factor $\log(1 - F_{B.U.})$ for the ^{19}F projectile was calculated using the empirical relation as Eq. (7) given by Wang *et al.* [54] and found to be $\approx$0.66:

$$\log(1 - F_{B.U.}) = -0.33 \exp(-0.29/E_{B.U.}) - 0.087 E_{B.U.}. \quad (7)$$

Figure 10 represents an exponential relation between the suppression factor in terms of the break-up threshold energy of the projectile. The suppression factor obtained by fitting and by Eq. (7) for the strongly bound projectile ^{19}F are presented in Fig. 10. As can be seen from this figure, the CF suppression factor for the ^{19}F projectile is found to be lower than for the weakly bound projectile ^{9}Be and higher than for the strongly bound projectile ^{10}B, which is related to the fact that the break-up threshold energy of ^{19}F is larger than that of ^{9}Be and smaller than that of ^{10}B. The present results for the ^{19}F projectile on different targets presented in Fig. 10 are found to be in good agreement with the systematics developed by Wang *et al.* [54] and show a well-established exponential relation between the CF suppression factor and the break-up threshold of the projectile. Further, the total fusion (TF) function for the same six systems was calculated for which the total fusion cross section ($\sigma_{TF} = \sigma_{CF} + \sigma_{ICF}$) could be measured and is presented
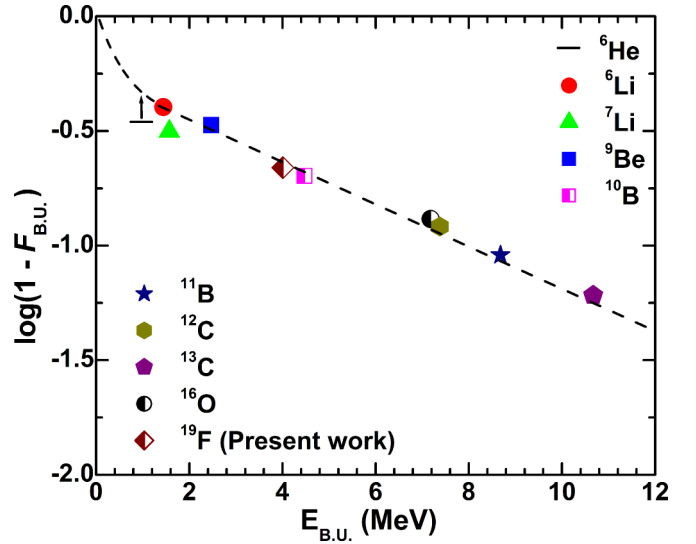

FIG. 10. The deduced suppression factor for the ^{19}F projectile is plotted as a function of the break-up threshold of the projectile. The dotted line represents the empirical Eq. (7) (for details see text).

in Fig. 11. As can be seen from this, the total fusion functions are found to be well matched with the UFF within statistical uncertainty, which means that there is no effect of break-up on the total fusion cross section.

D. Observation of incomplete fusion below ℓ_{crit}: Diffuseness in the ℓ distribution

As demonstrated in Ref. [30], the study of the ℓ distribution for the present system has been studied as well. The values of ℓ_{crit} for the ^{19}F + ^{175}Lu system is deduced using the prescription given in Ref. [55] and found to be 65$\hbar$. The fusion ℓ distribution for the CN formed in the interaction of the ^{19}F + ^{175}Lu system at the studied range of energies was
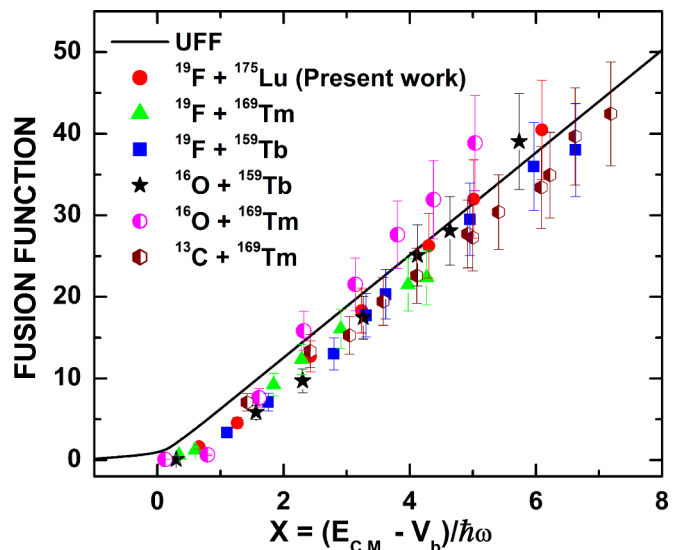

FIG. 11. The experimentally deduced total fusion functions for strongly bound projectiles on different target nuclei are compared with the UFF. The solid black curve is the UFF (for details see text).
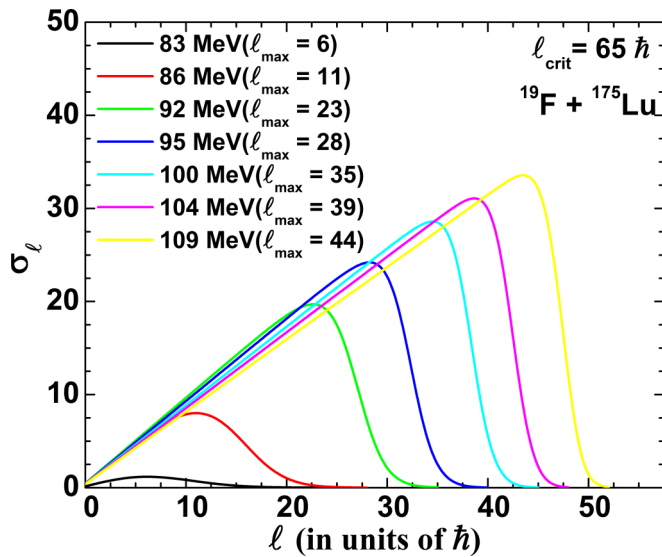
FIG. 12. Fusion ℓ distributions calculated using the code CCFULL to understand the population of ℓ bins at each studied energy.

calculated using the code CCFULL [56] and is presented in Fig. 12. As can be observed from Fig. 12, at the highest incident beam energy, $\ell_{max} < \ell_{crit}$, which suggests that a significant number of ℓ bins below ℓ_{crit} may contribute to the ICF process, indicating a diffused boundary for ℓ values, contrary to the sharp cutoff model, which may penetrate close to the barrier.

IV. SUMMARY AND CONCLUSIONS

In the present work, EFs of evaporation residues populated via CF and/or ICF processes in the interaction of ^{19}F + ^{175}Lu

were measured at energies ranging from $1.1V_b$ to $1.4V_b$ and are analyzed within the framework of the statistical model code PACE4. The EFs for the xn/pxn channels are well reproduced by the PACE4 code for the level density parameter $a = A/10$ MeV^{-1}, indicating their production solely via the CF. However, in the case of α-emitting channels, a significant enhancement in the production cross sections is observed when compared with PACE4 predictions even in the case of the non-α-cluster (^{19}F) beam. The observed enhancement indicates the onset of ICF reactions at energies above the Coulomb barrier. Further, in the present work, an attempt was made to see the break-up effects of strongly bound projectiles ^{13}C, ^{16}O, and ^{19}F with different target nuclei on fusion cross sections at energies above the barrier. The deduced experimental CF function has been compared within the framework of the universal fusion function, a benchmark curve. A significant CF suppression of about 10–35% was observed, which clearly manifests the prompt break-up of the projectile. The CF suppression in the case of ^{19}F as a projectile on various targets is found to be almost independent of the target charge. The deduced complete fusion suppression factor for the ^{19}F projectile shows an influential effect with respect to the break-up threshold energy of the projectile; i.e., the CF suppression is mainly determined by the break-up threshold of the projectile as suggested by Wang *et al.* [54].

[1] F. Schussler *et al.*, Nucl. Phys. A **584**, 704 (1995).

[2] E. Gadioli *et al.*, Nucl. Phys. A **641**, 271 (1998).

[3] A. Diaz-Torres and I. J. Thompson, Phys. Rev. C **65**, 024606 (2002).

[4] M. Dasgupta *et al.*, Nucl. Phys. A **787**, 144 (2007).

[5] P. P. Singh *et al.*, Phys. Rev. C **80**, 064603 (2009); **78**, 017602 (2008).

[6] U. Gupta *et al.*, Nucl. Phys. A **811**, 77 (2008), and references therein.

[7] A. Diaz-Torres, D. J. Hinde, J. A. Tostevin, M. Dasgupta, and L. R. Gasques, Phys. Rev. Lett. **98**, 152701 (2007).

[8] J. O. Newton *et al.*, Phys. Lett. B **586**, 219 (2004).

[9] H. C. Britt and A. R. Quinton, Phys. Rev. **124**, 877 (1961).

[10] D. P. Singh, Unnati, P. P. Singh, A. Yadav, M. K. Sharma, B. P. Singh, K. S. Golda, R. Kumar, A. K. Sinha, and R. Prasad, Phys. Rev. C **81**, 054607 (2010).

[11] A. Yadav *et al.*, Phys. Rev. C **96**, 044614 (2017), and references therein.

[12] T. Inumura *et al.*, Phys. Lett. B **84**, 71 (1979).

[13] T. Inumura *et al.*, Phys. Lett. B **68**, 51 (1977)

[14] R. Kauffmann and R. Wolfgang, Phys. Rev. **121**, 206 (1961).

[15] T. Udagawa and T. Tamura, Phys. Rev. Lett. **45**, 1311 (1980).

[16] E. Takada, T. Shimoda, N. Takahashi, T. Yamaya, K. Nagatani, T. Udagawa, and T. Tamura, Phys. Rev. C **23**, 772 (1981).

[17] J. Wilczynski *et al.*, Nucl. Phys. A **373**, 109 (1982).

[18] M. Blann, Phys. Lett. **27**, 337 (1971).

[19] J. P. Bondrof *et al.*, Nucl. Phys. A **333**, 285 (1980).

[20] B. G. Harvey, Phys. Lett. B **130**, 373 (1983).

[21] B. G. Harvey, Nucl. Phys. A **444**, 498 (1985)

[22] A. Y. Abul-Magd, Z. Phys. A **298**, 143 (1980).

[23] M. H. Simbel and A. Y. Abul-Magd, Z. Phys. A **294**, 277 (1980).

[24] Mohd. Shuaib *et al.*, Phys. Rev. C **94**, 014613 (2016), and references therein.

[25] U. Gupta *et al.*, Phys. Rev. C **80**, 024613 (2009).

[26] Manoj Kumar Sharma *et al.*, Nucl. Phys. A **776**, 83 (2006).

[27] V. R. Sharma *et al.*, Nucl. Phys. A **946**, 182 (2016), and references therein.

[28] A. Gavron, Phys. Rev. C **21**, 230 (1980).

[29] L. F. Canto *et al.*, Nucl. Phys. A **821**, 51 (2009), and references therein.

[30] Mohd. Shuaib *et al.*, J. Phys. G: Nucl. Part. Phys. **44**, 105108 (2017), and references therein.

[31] N. G. Puttaswamy *et al.*, Proc. DAE Symp. **34B**, 405 (1991).

[32] B. P. Ajith Kumar *et al.*, CANDLE: Collection and Analysis of Nuclear Data using Linux nEtwork, Proc. DAE Symp. **44B**, 390 (2001).

[33] A. Sood *et al.*, Phys. Rev. C **96**, 014620 (2017), and references therein.

[34] E. Browne and R. B. Firestone, *Table of Radioactive Isotopes* (Wiley, New York, 1996).

[35] J. K. Tuli, *Nuclear Wallet Card, National Nuclear Data Center* (Brookhaven National Laboratory, Upton, New York, USA, 1995).

[36] B. P. Singh, Ph.D. thesis, Aligarh Muslim University, Aligarh, India, 1991 (unpublished).

[37] W. Hauser and Hi Feshbach, Phys. Rev. **87**, 366 (1952).

[38] A. Gilbert and A. G. W. Cameron, Can. J. Phys. **43**, 1446 (1965).

[39] S. K. Kataria, V. S. Ramamurthy, and S. S. Kapoor, Phys. Rev. C **18**, 549 (1978); **19**, 297(E) (1979).

[40] R. Bass, Nucl. Phys. A **231**, 45 (1974).

[41] F. D. Becchetti and G. W. Greenless, Phys Rev. **182**, 1190 (1969).

[42] G. R. Satchler, Nucl. Phys. A **70**, 177 (1965).

[43] M. Cavinato, E. Fabrici, E. Gadioli, E. Gadioli Erba, P. Vergani, M. Crippa, G. Colombo, I. Redaelli, and M. Ripamonti, Phys. Rev. C **52**, 2577 (1995).

[44] R. D. Evans, *The Atomic Nucleus* (McGraw-Hill, Bombay, 1995).

[45] J. R. Leigh *et al.*, Phys. Rev. C **52**, 3151 (1995).

[46] J. Zhang *et al.*, Nucl. Phys. A **864**, 128 (2011).

[47] P. R. S. Gomes *et al.*, Nucl. Phys. A **834**, 151c (2010), and references therein.

[48] M. Beckerman, M. Salomaa, A. Sperduto, J. D. Molitoris, and A. DiRienzo, Phys. Rev. C **25**, 837 (1982).

[49] P. R. S. Gomes, J. Lubian, I. Padron, and R. M. Anjos, Phys. Rev. C **71**, 017601 (2005).

[50] L. F. Canto *et al.*, J. Phys. G: Nucl. Part. Phys. **36**, 015109 (2009)

[51] R. Wolski, Phys. Rev. C **88**, 041603(R) (2013).

[52] V. R. Sharma *et al.*, AIP Conf. Proc. **1524**, 201 (2013).

[53] V. R. Sharma *et al.*, Phys. Rev. C **89**, 024608 (2014).

[54] B. Wang *et al.*, Phys. Rev. C **90**, 034612 (2014).

[55] J. Wilczynski *et al.*, Phys. Lett. **45**, 606 (1980).

[56] K. Hagino, N. Rowley, and A. T. Kruppa, Comput. Phys. Commun. **123**, 143 (1999).